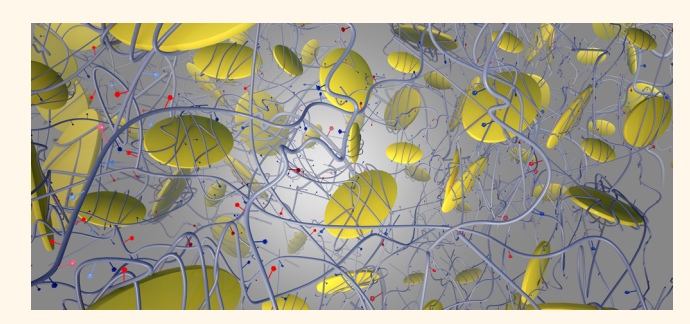
# Bioactive Nanoengineered Hydrogels for Bone Tissue Engineering: A **Growth-Factor-Free Approach**

- Janet R. Xavier, Teena Thakur, Prachi Desai, Manish K. Jaiswal, Nick Sears,
- Elizabeth Cosgriff-Hernandez, †,‡ Roland Kaunas,† and Akhilesh K. Gaharwar\*,†,‡
  - Department of Biomedical Engineering and Department of Materials Science and Engineering, Texas A&M University, College Station, Texas 77843, United States

ABSTRACT Despite bone's impressive ability to heal after traumatic injuries and fractures, a significant need still exists for developing strategies to promote healing of nonunion defects. To address this issue, we developed collagen-based hydrogels containing two-dimensional nanosilicates. Nanosilicates are ultrathin nanomaterials with a high degree of anisotropy and functionality that results in enhanced surface interactions with biological entities compared to their respective three-dimensional counterparts. The addition of nanosilicates resulted in a 4-fold increase in compressive



modulus along with an increase in pore size compared to collagen-based hydrogels. In vitro evaluation indicated that the nanocomposite hydrogels are capable of promoting osteogenesis in the absence of any osteoinductive factors. A 3-fold increase in alkaline phosphatase activity and a 4-fold increase in the formation of the mineralized matrix were observed with the addition of the nanosilicates to the collagen-based hydrogels. Overall, these results demonstrate the multiple functions of nanosilicates conducive to the regeneration of bone in nonunion defects, including increased network stiffness and porosity, injectability, and enhanced mineralized matrix formation in a growth-factor-free microenvironment.

KEYWORDS: nanocomposite hydrogels · tissue engineering · synthetic nanosilicates · scaffolds · two-dimensional (2D) nanoparticles · bone regeneration

anocomposite hydrogels are emerging biomaterials used for a range of tissue engineering approaches.<sup>1–5</sup> Hydrogels are able to mimic some of the physical and chemical properties of the extracellular matrix (ECM) due to their structural similarity to native tissue. By adding different nanoparticles, including graphene, graphene oxide, carbon nanotubes (CNTs), hydroxyapatite (nHAp), bioactive glasses, and calcium phosphate, the mechanical and biological characteristics of nanocomposite hydrogels can be enhanced.<sup>6–8</sup> Most of these nanoparticles have been shown to support cell adhesion and proliferation, and only a few have been shown to influence cell differentiation.

Recently, we reported two-dimensional (2D) nanosilicates with a high degree of anisotropy and functionality for biomedical applications. 9-12 The recent rapid advances in 2D nanoparticle technologies have raised exciting questions about their interactions

with biological moieties.3-5 The addition of 2D nanosilicates to human mesenchymal stem cells (hMSCs)<sup>9</sup> and adipose stem cells (ASCs)<sup>10</sup> was shown to induce osteogenic differentiation without the use of dexamethasone, bone morphogenic protein-2 (BMP-2), or other growth factors. Nanosilicate (Laponite, Na<sup>+</sup><sub>0.7</sub>[(Mg<sub>5.5</sub>Li<sub>0.3</sub>)Si<sub>8</sub>O<sub>20</sub>-(OH)<sub>4</sub>]<sup>-</sup><sub>0.7</sub>) is a hydrous sodium lithium magnesium silicate. The degradation products of nanosilicates are magnesium, orthosilicic acid, and lithium, which can be easily absorbed by the body and are individually shown to have properties that are potentially useful for bone tissue engineering.<sup>13</sup> For example, lithium, an FDA-approved inhibitor of glycogen synthetase kinase-3 $\beta$  (GSK3 $\beta$ ), activates Wntresponsive genes by elevating cytoplasmic  $\beta$ -catenin. 14,15 Orthosilicic acid (Si(OH)<sub>4</sub>) promotes collagen type I synthesis and osteoblast differentiation via the WNT/  $\beta$ -catenin signaling pathway. The role of

\* Address correspondence to gaharwar@tamu.edu (A. K. Gaharwar).

Received for review December 31, 2014 and accepted February 12, 2015.

**Published online** 10.1021/nn507488s

© XXXX American Chemical Society

www.acsnano.org

9

10

11

12

13

15

16

17

19

20

21

22

23

24

25

26

27

28

29

30

31

32

33

35

36

40

44

45

46

47

48

49

50

51

52

53

112

113

114

115

116

117

118

119

120

121

122

123

124

125

126

127

128

129

130

131

132

133

134

135

136

137

138

139

140

141

142

143

144

145

146

147

148

149

150

151

152

153

154

155

156

157

158

159

160

161

162

163

164

165

166

Wnt signaling has been implicated in osteogenic differentiation of stem cells. <sup>16</sup> Moreover, nanocomposite hydrogels loaded with nanosilicates are biocompatible and biodegradable under *in vivo* conditions <sup>11</sup> and can be used for a range of biomedical and biotechnological applications.

54

55

56

57

58

59

60

61

62

63

64

65

66

67

68

69

70

71

72

73

74

75

76

77

78

79

80

81

82

83

84

85

86

87

88

89

90

91

92

93

94

95

96

97

98

99

100

101

102

103

104

105

106

107

108

109

110

Compared to other types of 2D nanoparticles such as graphene or graphene oxide (GO), nanosilicates have been shown to provide enhanced physical, chemical, and biological functionality due to a discotic charged surface, uniform shape, high surface-to-volume ratio, and biocompatible nature. 1-5 The presence of both positive and negative charges on the nanosilicate surface results in unique anisotropic interactions between the nanoparticles that generate new unconventional phases at the nano- and microscales. 17-19 This allows nanosilicates to interact with anionic, cationic, and neutral polymers to form a physically cross-linked network with shear-thinning characteristics. 11,12,20 The uniform shape of nanosilicates compared to GO provides additional control over the interactions between nanoparticles and polymer chains to develop multifunctional biomaterials.<sup>3,5</sup> Moreover, the optical transparency of nanosilicates 17 in aqueous media compared to GO permits imaging of the subsurface cellular process to design complex tissue structures.

In this study, we developed an injectable osteoinductive collagen-based nanosilicate matrix for growth-factor-free bone tissue engineering. Natural hydrogel-forming polymers such as collagen are able to mimic native tissue-like properties due to the presence of cell-binding domains Arg-Gly-Asp (RGD) and can be easily modified to obtain covalently crosslinked hydrogels with native tissue-like mechanical properties.<sup>21–24</sup> The unique shape and surface charge of nanosilicates promote strong interactions with a collagen-based matrix (gelatin) to form self-assembled structures, which can dynamically form and break to result in shear-thinning properties. Upon UV exposure, the self-assembled structures of a collagen-based matrix and nanosilicates form a highly cross-linked and vstable network (Figure 1a). We hypothesize that incorporating nanosilicates within a collagen-based matrix will provide control over the physical properties of the hydrogel network due to enhanced interactions between the nanosilicates and gelatin backbone. Moreover, the ability of a collagen-based hydrogel loaded with nanosilicate to promote mineralized matrix formation in a growth-factor-free microenvironment for regeneration of bone is unique. Given that the treatment of bone defects remains one of the largest challenges in musculoskeletal tissue engineering, our nanocomposite hydrogel represents a new material design in the broadly interesting area of growth-factorfree strategies. Overall, these dynamic and bioactive nanocomposite gels show strong promise in bone tissue engineering applications.

#### **RESULTS AND DISCUSSION**

Nanosilicate - Gelatin Interactions. Nanosilicate (Laponite,  $Na^{+}_{0.7}[(Mg_{5.5}Li_{0.3})Si_{8}O_{20}(OH)_{4}]^{-}_{0.7})$  is a hydrous sodium lithium magnesium silicate characterized by a high aspect ratio (20-40 nm in diameter and 1 nm in thickness) (Figure 1b). Due to the unique crystal structure and charged surface of nanosilicates, a strong physical interactions between a nanosilicate and polyampholytic gelatin was expected. Gelatin is denatured collagen and mimics components of the native extracellular matrix in structure and chemical composition. To fabricate covalently cross-linked hydrogels, amine groups present on the gelatin backbone were replaced by a methacrylate group to obtain gelatin methacrylate (GelMA) according to previously published reports.<sup>21–24</sup> The interactions between a nanosilicate and a prepolymer (GelMA) were investigated using electrophoresis and transmission electron microscopy (TEM). The zeta potential of GelMA and the nanosilicates was observed to be  $-11.3 \pm 0.4$  and  $-28 \pm 3$  mV, respectively. With the addition of nanosilicates to GelMA, a decrease in zeta potential was observed (Figure 1c). Specifically, the addition of 0.5, 1, and 2% nanosilicates to GelMA resulted in a decrease in the zeta potential of the nanocomposites to  $-13 \pm 2.6$ ,  $-33.4 \pm 2.9$ , and  $-34.4 \pm 0.9$  mV, respectively. The decrease in the zeta potential of nanocomposites indicates that nanosilicates strongly interact with gelatin at nanosilicate concentrations ≥ 1%. Additionally, our earlier results also indicate that nanosilicates are uniformly dispersed within the gelatin network without any aggregation.11

The shear-thinning characteristics of the prepolymer solutions containing GelMA and GelMA-2% nanosilicates were determined by monitoring viscosity at different shear rates at 37 °C (Figure 1d). The prepolymer solution (5 wt % GelMA) was a liquid at 37 °C, and the addition of nanosilicates significantly increased the viscosity of the solution with nanosilicate concentrations higher than 2%, resulting in a semisolid that needed skilled handling with smaller diameter pipets. The unique shape and surface charge distribution on the nanosilicates provide a significantly higher surface-to-volume ratio compared to other types of nanoparticles. Moreover, due to the presence of both positive and negative charge on the nanosilicates, it results in the formation of a house-of-cards structure and exhibits a shear-thinning characteristic. 17-19

Covalently Cross-Linked Nanocomposite Hydrogels. We fabricated a covalently cross-linked gelatin hydrogel (Gel) by exposing a prepolymer solution of GelMA to UV radiation in the presence of a photoinitiator. By adding 0.5, 1, and 2 wt % of nanosilicates to GelMA, covalently cross-linked nanocomposite hydrogels were fabricated for physical and biological characterization. The addition of nanosilicates provided a desired combination of tunable structure and bioactivity characteristics.

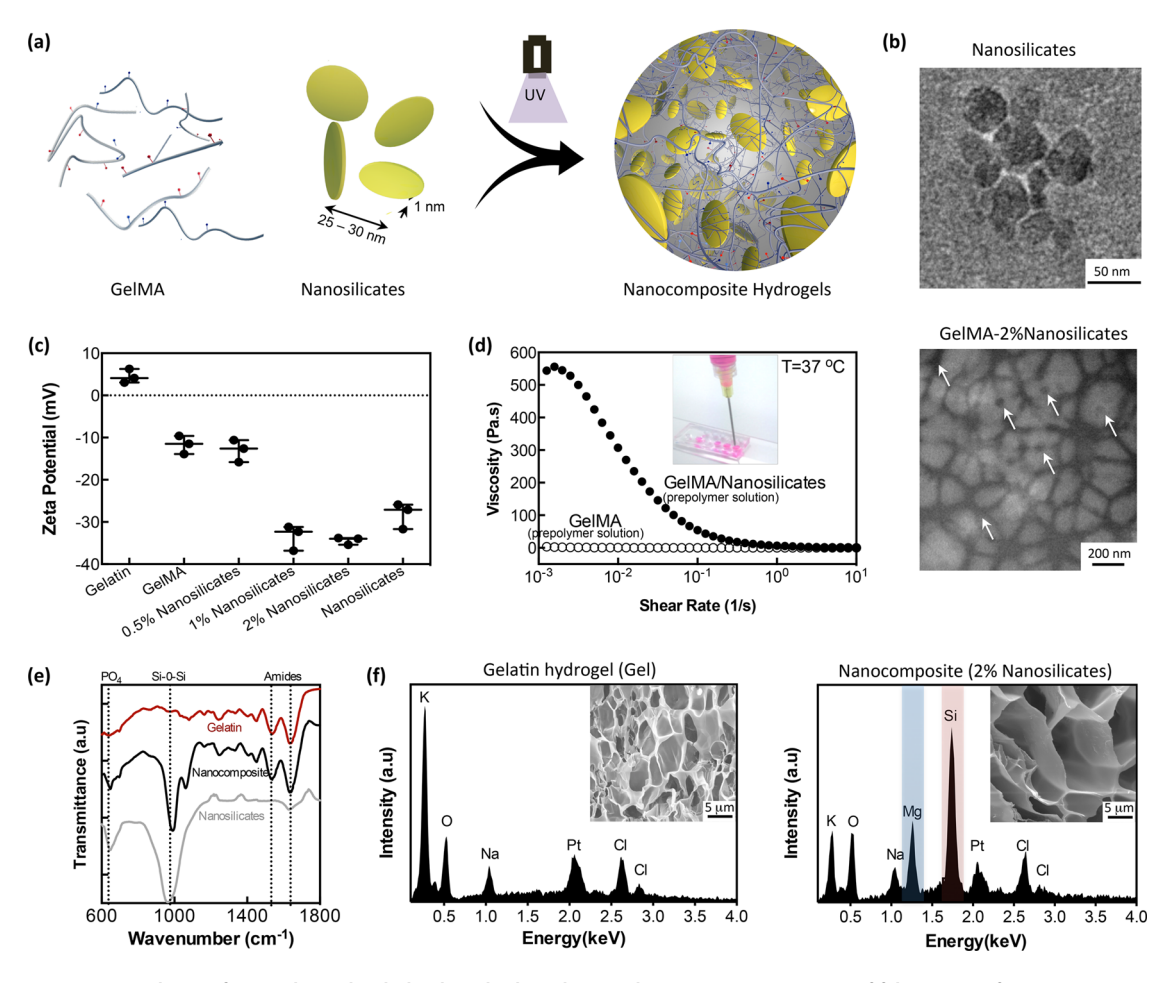


Figure 1. Synthesis of nanosilicate-loaded gelatin hydrogels. (a) Schematic representation of fabrication of nanocomposite hydrogels from GelMA (prepolymer) and nanosilicates by covalent cross-linking under UV radiation. (b) TEM image showing the size and morphology of nanosilicates with an average diameter of 20–30 nm. Nanosilicates were uniformly distributed within a nanocomposite network (2% silicate), and no aggregation was observed (arrows indicate nanosilicates). (c) The interactions between silicates and gelatin were investigated by monitoring zeta potential. (d) Viscosity—shear rate of prepolymer solution (GelMA and GelMA loaded with nanosilicates) highlights shear-thinning characteristic of the prepolymer solution loaded with nanosilicates. (e) FTIR spectra of nanocomposite hydrogel's structure showed the presence of a Si–O–Si peak (960 cm<sup>-1</sup>) and amides in the nanocomposite hydrogel upon cross-linking. (f) The addition of silicate nanoparticles increased the hydrogel porosity due to enhanced interactions with the polymeric chains (inset). The EDX spectra of a covalently cross-linked gelatin hydrogel (Gel) and a nanocomposite hydrogel indicated the presence of Si and Mg in the nanocomposite, but not in Gel.

The presence of nanosilicates within the gelatin network after the cross-linking process was confirmed *via* infrared (IR) spectra, as shown in Figure 1e. The peak near 960 cm<sup>-1</sup> observed in the nanosilicates was due to stretching of Si–OH and Si–O and bending of Si–O–Si bonds present in the nanosilicates. Gelatin showed prominent amine peaks near 1540 and 1650 cm<sup>-1</sup>. The nanocomposites contained both Si–OH and amine peaks, indicating the presence of both gelatin and nanosilicates.

The hydration properties of nanocomposite hydrogels are important to investigate, as the diffusion of nutrients and waste products strongly depends on the hydration degree.<sup>25</sup> Moreover, changing the hydration degree can alter cellular infiltration during *in vivo* implantation. The hydration degree of nanocomposites was quantifed in different medium compositions, including PBS and cell culture media (DMEM and

DMEM + 10% FBS) (Figure S1). The addition of nanosilicates reduced the hydration degree, likely due to strong interactions between gelatin and nanosilicates. Performing the assays with PBS at different pH levels or with culture media instead of PBS did not significantly alter the results.

The porosity of tissue-engineered scaffolds plays an important role in directing cellular behavior, as the size and distribution of pores within scaffolds dictate the cellular infiltration and distribution of cells throughout the network. <sup>25</sup> Gel hydrogels showed a uniform and highly interconnected network, similar to previously published literature. <sup>21,26</sup> The addition of nanosilicates to Gel resulted in an increase in pore size of the covalently cross-linked network (Figure 1f and Figure S2). The Gel hydrogel displayed pore sizes between 0.2 and 0.9  $\mu$ m, which substantially increased to 0.3–1.5  $\mu$ m with the incorporation of 2% nanosilicates. This finding

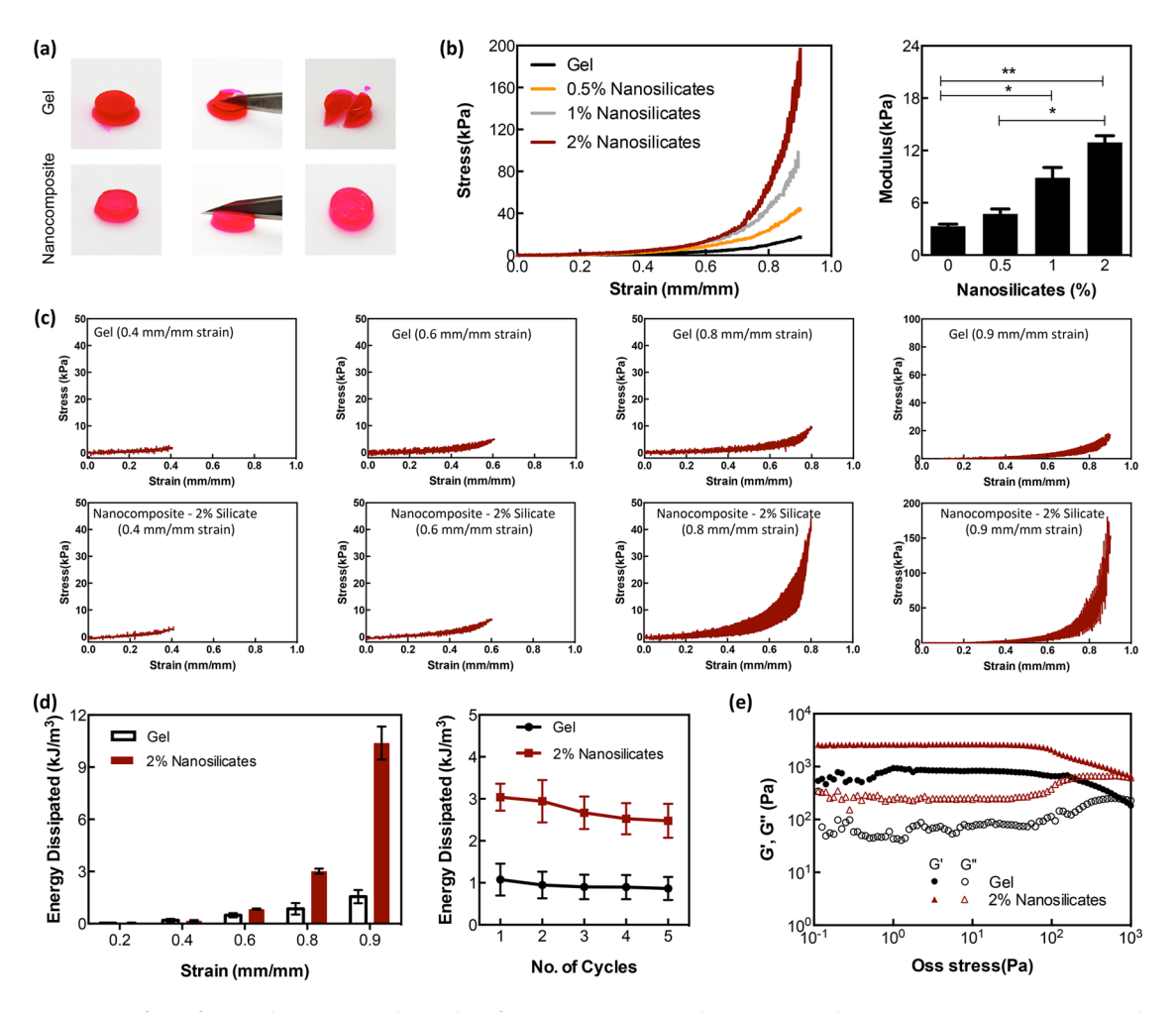


Figure 2. Effect of nanosilicate on mechanical stiffness was investigated using uniaxial compression testing. (a) Optical images showing mechanical toughness of the Gel and nanocomposite hydrogels (2% nanosilicates) after deformation. (b) Nanocomposite hydrogels were subjected to unconfined compression up to 0.90 strain. From the stress—strain curves, the compressive modulus of the hydrogels was calculated from the 0.10-0.20 strain (toe region) (\*p < 0.05, \*\*p < 0.01). (c) Nanocomposite hydrogels were subjected to cyclic compression of amplitude ranging from 0.20 to 0.90 strain. (d) Energy dissipation calculated from the observed hysteresis with different strain. Effect of number of cycles on energy dissipation at 0.8 strain from the Gel and nanocomposites with 2% nanosilicates. (e) Oscillatory rheometric analysis indicates frequency-dependent changes in the elastic (G') and loss (G'') moduli.

is interesting in that it differs from the existing reports related to most other nanocomposite materials, in which physical reinforcement of the polymeric network by nanoparticles results in smaller pore size. 27,28 In the nanocomposites, the increase in the pore size may be attributed to the enhanced interactions between the nanosilicates and the gelatin, which locally condense the polymer fraction to result in the formation of larger voids. The microscopic images confirmed the uniform dispersion of nanoparticles within the polymer network with no visible aggregates. A further analysis with energy-dispersive X-ray spectroscopy (EDS) also indicated the presence of silicon (Si) and magnesium (Mg) in the nanocomposites, indicating their presence in the porous structure (Figure 1f).

Nanosilicates Enhance Mechanical Stiffness. Nanosilicates interacted with the polymeric matrix to increase the mechanical stiffness. Figure 2a shows that the Gel hydrogel readily broke when compressed with a sharp

object, whereas the addition of 2D nanosilicates significantly improved the network stability under stress. To quantify the effects of nanosilicates on the mechanical stiffness, hydrogel samples were subjected to uniaxial compression testing. The Gel hydrogel showed an increase in stress with an increase in strain (Figure 2b). The modulus calculated from the initial linear region (0.1-0.2 mm/mm strain) of the Gel stress-strain curve was observed to be 3.3  $\pm$  0.4 kPa, which is comparable to previously published reports. 26,29 The addition of small amounts of nanosilicates showed a significant increase in compressive modulus. For example, the addition of 0.5, 1, and 2% nanosilicates resulted in an increase in modulus to 4.7  $\pm$  0.9, 8.9  $\pm$  2.1, and 12.9  $\pm$  1.3 kPa, respectively. The 4-fold increase in compressive modulus due to the addition of 2% nanosilicates can be attributed to enhanced nanoparticle polymer interactions. A 10-fold increase in peak tensile stress at 90% strain was also observed upon

222

223

224

225

226

227

228

229

230

231

232

233

234

235

236

237

238

239

240

203

204

205

206

207

208

209

210

211

212

213

214

215

216

217

218

219

221

**F2** 220

299

300

301

302

303

304

305

306

307

308

309

310

311

312

313

314

315

316

317

318

319

320

321

322

323

324

325

326

327

328

329

330

331

332

333

334

335

336

337

338

339

340

341

342

343

344

345

346

347

348

349

350

351

352

353

354

addition of nanosilicates with the Gel displaying a stress of 16  $\pm$  2.9 kPa and the nanocomposite containing 2% nanosilicates displaying a stresss of 164  $\pm$  30 kPa.

241

242

243

244

245

246

247

248

249

250

251

252

253

254

255

256

257

258

259

260

261

262

263

264

265

266

267

268

269

270

271

272

273

274

275

276

277

278

279

280

281

282

283

284

285

286

287

288

289

290

291

292

293

294

295

296

297

To further investigate the effect of nanosilicates on the elastomeric properties of hydrogels, cyclic compression testing was performed consisting of five cycles of loading and unloading. The energy dissipated during cyclic loading was calculated from the area under the stress-strain curves over a range of strain amplitudes (Figure 2c). Hysteresis became apparent for strains above 0.40, indicating absorption of energy during deformation. Consistent with the results from a single loading (Figure 2b), the maximum stress at each strain amplitude was significantly higher for nanocomposites compared to the Gel hydrogels. The energy absorbed during the deformation (90% cyclic compression) of the Gel and nanocomposite containing 2% nanosilicates was 1.5  $\pm$  0.4 and 10.4  $\pm$ 2.3 kJ/m<sup>3</sup>, respectively (Figure 2d). The addition of 2% nanosilicates to the Gel resulted in a greater than 6-fold increase in energy absorbed by the network. The increased energy dissipation is due to the relatively high stress generated with the stiffer nanocomposite. Furthermore, the curves were repeatable after multiple cycles of loading and unloading, demonstrating that no plastic deformation was detected (Figure 2d). Thus, nanocomposites are each highly elastic under high compressive strains.

The effects of the addition of nanosilicates to the Gel network on gel rheology were investigated by subjecting the hydrogels to a range of amplitudes of oscillatory shear stress to calculate the elastic storage (G') and loss (G'') moduli (Figure 2e). Each hydrogel showed significantly higher G' compared to G'' at all shear stress amplitudes tested. Consistent with the results of the compression testing, the addition of nanosilicates increased G'.

In contrast, other types of nanoparticles incorporated within Gel hydrogels display minimal increases in modulus. For example, Shin et al. incorporated 5 mg/mL of multiwalled carbon nanotubes functionalized with carboxyl groups within Gel hydrogels,<sup>26</sup> and no significant increase in compressive modulus was observed. In a similar study, the addition of graphene oxide into Gel hydrogels did not significantly change the compressive modulus for a given UV exposure time.<sup>29</sup> These studies indicated that these nanoparticles act simply as fillers that did not increase the mechanical stiffness of the hydrogel network.<sup>26,29</sup> However, covalent cross-linking of nanoparticles to polymer chains can significantly increase stiffness. For example, Cha et al. observed that 3 mg/mL of methacrylated graphene oxide conjugated to the Gel resulted in a 2- to 3-fold increase in stiffness.<sup>30</sup> In the current study, the addition of nanosilicates to the Gel increased the stiffness by more than 4-fold through

noncovalent interactions between the nanosilicates and the Gel. Although the exact interactions between the Gel and nanosilicates are yet to be fully established, it can be expected that free amine and carboxylic groups present on the Gel backbone might interact with the charged surface of the nanosilicates.

Nanosilicates Enhance in Vitro Biomineralization and Physiological Stability. In vitro biomineralization, which involves the deposition of hydroxyapatite in the presence of stimulated body fluid (SBF), can be used to evaluate the in vitro osteogenic bioactivity of the hydrogel network.31 When a biomaterial's surface is submerged in SBF, the formation of apatite-like deposits on the biomaterial surface indicates the bone-bonding capability of the hydrogel network. Collagen is one of the major components of bone and induces the nucleation of hydroxyapatite crystals.<sup>32</sup> In our study, scanning electron microscopy (SEM) and energydispersive X-ray spectroscopy (EDX) data clearly indicated the formation of mineralized deposits over the surface of both the Gel and nanocomposites (Figure S3a). Images of these materials stained with Alizarin Red S to identify calcium deposition indicated staining intensity increased with increasing nanosilicate concentration (Figure S3b). Alizarin Red S was extracted with acetic acid and quantified by colorimetric detection.<sup>33</sup> The results indicate a nanosilicate dosedependent increase of more than 50% in Alizarin Red S staining. These results suggest that nanosilicates provide additional sites for hydroxyapatite nucleation and growth.

Gelatin is a biodegradable polymer and is highly susceptible to enzymatic degradation. The enzymatic degradation rates of nanosilicate-reinforced Gel hydrogels were evaluated in vitro under accelerated degradation conditions by using 2.5 units/mL of a collagenase solution (at 37 °C). Gel hydrogels readily degraded in the presence of collagenase, with full dissolution occurring within 10-12 h (Figure S4a and b), consistent with previous reports. 21,29,30 Due to the highly interconnected and porous network (Figure S2), the collagenase solution can easily permeate the hydrogel network and degrade the entire network uniformly and rapidly. The addition of nanosilicates to the gelatin network significantly improved the stability of the hydrogel network under enzymatic conditions. The nanocomposite hydrogels containing 0.5, 1, and 2% nanosilicates degraded completely in approximately 50, 70, and 90 h, respectively. By fitting a first-order degradation (one-phase decay) curve to these results, the half-life of the Gel was observed to be 3.4 h, and the addition of 0.5, 1, and 2% nanosilicates improved the high-life of the network to 9.1, 18.5, and 22.9 h (Figure S4c). The more than 6-fold increase in the physiological stability of Gel hydrogels upon addition of 2% nanosilicates is likely due to the strong interactions between the polymer and nanoparticles.

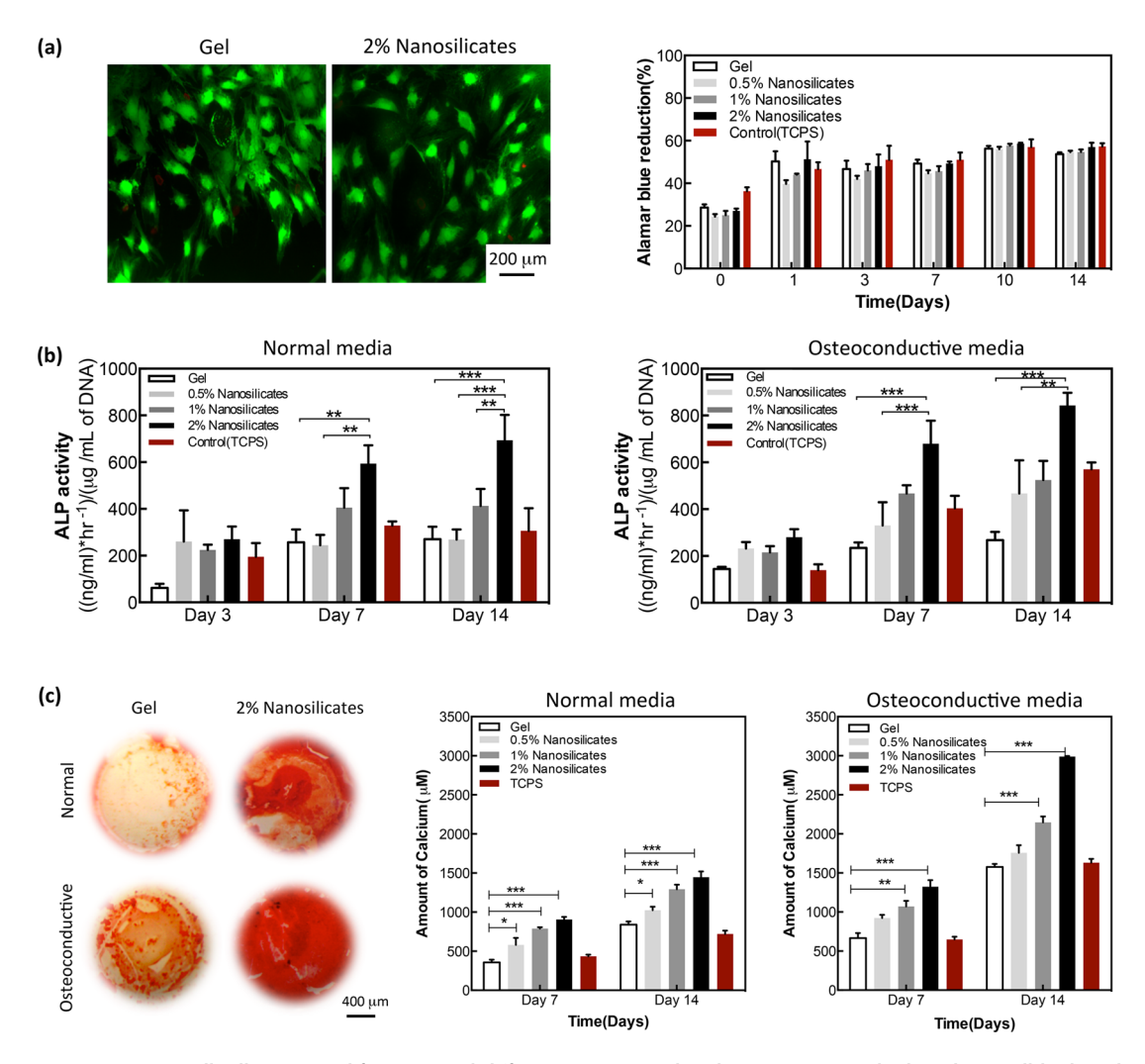


Figure 3. In vitro cell adhesion, proliferation, and differentiation on Gel and nanocomposite hydrogels. (a) All hydrogels supported initial cell adhesion/spreading (day 3) and proliferation, as determined by live/dead imaging and Alamar Blue assay of cells seeded on hydrogel surfaces. TCPS acted as the positive control. (b) The ALP activity was quantified and normalized with the amount of dsDNA present on days 3, 7, and 14. The addition of nanosilicates significantly upregulated ALP activity in both normal and osteocondutive media. (c) Inorganic calcium deposited by preosteoblast cells in normal and osteoconductive media was identified using Alizarin Red S staining. The optical images show the deposition of the mineralized matrix (stained red) on day  $14 \ (*p < 0.05, **p < 0.01, ***p < 0.001)$ .

The nanosilicate may act as a multifunctional crosslinker that interacts with multiple gelatin chains and potentially mask cleavage sites from collagenases.

Nanocomposites Support Cellular Adhesion and Enhance in Vitro Mineralization. The ability to support initial cell adhesion and subsequent proliferation is an important requirement of a tissue-engineered scaffold. Gelatin is a denatured protein that contains RGD groups, which play a significant role in cell adhesion via integrins. MC3T3 preosteoblasts were used to investigate the effect of nanosilicates on initial cell adhesion and proliferation. The cells readily adhered to Gel, and the addition of nanosilicates did not result in any significant influence in initial cell adhesion (Figures 3a and S5a). The cellular morphology indicated that the nanocomposites are cytocompatible and did not elicit any cytotoxic effects. The metabolic activity of preosteoblasts on the scaffold was quantified as a measure of

cell proliferation over a period of 14 days in both normal and osteoconductive media (Figures 3a and S5b). All nanocomposites supported cellular proliferation, and cells showed metabolic activity over a period of 14 days similar to cells cultured on conventional tissue culture polystyrene (TCPS) dishes. These results support our previous published results that indicate that nanosilicates are cytocompatible. Moreover, subcutanious implantation of nanosilicate—gelatin showed a locally restricted inflammatory reaction in the host and was completely degraded within 28 days under *in vivo* conditions. On the basis of these studies, nanosilicate-based hydrogels can be easily used for biomedical applications.

Specific biochemical and physical cues in the ECM play a critical role in regulating cellular processes and their fate. By controlling these cues in the engineered ECM, it is possible to regulate or enhance outcomes

s 390

F3 368

449

450

451

452

454

456

457

458

459

460

461

462

463

464

465

466

467

468

469

470

471

473

474

475

476

477

478

479

480

481

482

483

484

485

486

487

488

489

490

491

492

493

494

495

496

497

498

499

500

501

502

503

455 **F4** 

that facilitate tissue regeneration. To this end, the effects of nanosilicates on early osteogenic responses were monitored by qualitative and quantitative assessment of the presence and activity of ALP as an early marker of differentiation. We investigated the effect of nanosilicates on intracellular ALP production on days 3, 7, and 14 in both growth and osteoconductive media (growth media supplemented with 10 mM  $\beta$ -glycerophosphate and 50  $\mu$ M ascorbic acid phosphate) (Figure S6). In growth media, cells seeded on the nanocomposites displayed a higher level of ALP staining (purple stain) compared to Gel and TCPS on days 3, 7, and 14. A significantly higher amount of ALP staining was observed using the osteoconductive media. The increase in nanosilicate concentration was also evident on ALP staining, indicating the key role of nanosilicate in the upregulation of osteogenic differentiation.

391

392

393

394

395

396

397

398

399

400

401

402

403

404

405

406

407

408

409

410

411

412

413

414

415

416

417

418

419

420

421

422

423

424

425

426

427

428

429

430

431

432

433

434

435

436

437

438

439

440

441

442

443

444

445

446

447

The ALP activity was then quantified with a colorimetric assay to quantify the ability of nanosilicates to promote osteogenic differentiation (Figure 3b). The results indicated a nanoparticle dose-dependent increase in ALP activity, with the addition of 2% nanosilicates causing a greater than 2.5-fold increase in ALP activity on day 14 compared to cells seeded on the Gel. There was no difference in the ALP activity of cells seeded on the Gel and TCPS on day 14, indicating that these materials are not osteoinductive. Importantly, the addition of 1% and 2% nanosilicates was able to significantly enhance the ALP activity in the growth media in the absence of any supplements (beta glycerol phosphates and ascorbic acid). A similar nanosilicate dose-dependent increase in ALP activity was detected in the presence of osteoconductive media, with the absolute ALP activities increased relative to that in growth media.

The production of bone-like inorganic calcium deposits, a hallmark for late-stage osteogenic differentiation, was determined by Alizarin Red S staining (Figures 3c and S7). While red staining was observed in all compositions, significant increases were seen in the nanocomposites. A summary of the results from quantitative analysis of Alizarin Red S extracts shows a dosedependent increase in calcium in the mineralized matrix produced by cells seeded on the nanocomposites on days 7 and 14 (Figure 3c). Further, there was clearly greater calcium deposition in the osteoconductive media. The deposition of hydroxyapatite in nanocomposite hydrogels was confirmed by Raman spectra (Figure S8). The presence of a very strong PO<sub>4</sub> peak at 961 cm<sup>-1</sup> indicates the presence of hydroxyapatite in nanocomposite hydrogels. It is important to note that these assays were performed in the absence of osteogenic factors such as dexamethasone and bone morphogenic protein. Thus, the extent of mineralization from the Alizarin Red S staining showed that nanosilicates promoted osteogenic differentiation of preosteoblast cells and the mineralization of ECM in both

normal and osteoconductive media in the absence of any osteogenic factors.

To further evaluate the potential of nanosilicatebased hydrogels for tissue engineering, we evaluated the ability to engineer intrinsic structure with a welldefined microenvironment. We engineered microgels (<600 µm diameter) from Gel-nanosilicate hydrogels using photolithography (Figure 4a). The cells seeded on these microfabricted structures readily adhered and spread on the surface of the hydrogels. The cells stained for actin filaments (red) and nuclei (blue) exhibited elongated morphology and the formation of an interconnected network. The encapsulated cells within the hydrogel network showed high cytocompatibility, as shown by live/dead staining after day 1, day 2, and day 4 (Figure 4b). This indicates that the bioactive nanosilicate-based hydrogel construct can be used to encapsulate cells without adversely affecting cellular viability.

A major challenge for 3D printing of biopolymers is maintaining mechanical integrity and preventing pore collapse while building the construct.<sup>34</sup> Reasonable improvements in printing quality have been made by including hyaluronan or using precise control of the deposition head and substrate temperatures.<sup>35</sup> However, these constructs required high concentrations (10–20 wt %) of gelatin to create viable scaffolds. In contrast, the shear-thinning characteristic of the Gel-nanosilicate microgels enables the printing of precisely designed scaffolds (Figure 4c). Solutions without nanosilicates did not retain dimensional features after printing. This indicates that the nanosilicatebased hydrogels can be used as bioinks for printing complex structures for tissue repair and organ replacement. Our future work in this direction will involve the encapsulation of human bone marrow derived stem cells within the 3D nanosilicate-based hydrogels for functional tissue and organ replacement strategy.

### CONCLUSION

We engineered bioactive nanocomposite hydrogels loaded with nanosilicates within collagen-based polymer networks. Although the use of nanosilicates in the life sciences is still in its infancy, the promising bioactive effects promoted by interactions with nanosilicates has opened a wide range of biomedical and biological applications, including therapeutics, imaging, and disease-related diagnostics for regenerative medicine. When incorporated into a gelatin matrix, the nanosilicates likely interact with polymeric chains through strong electrostatic interactions and were shown to enhance several physical, chemical, and biological properties of the hydrogel. The addition of silicate nanoparticles increased stiffness and in vitro enzymatic stability, thus improving the tunable mechanical properties and degradation profile. In vitro data indicated that silicate-based bioactive nanocomposites

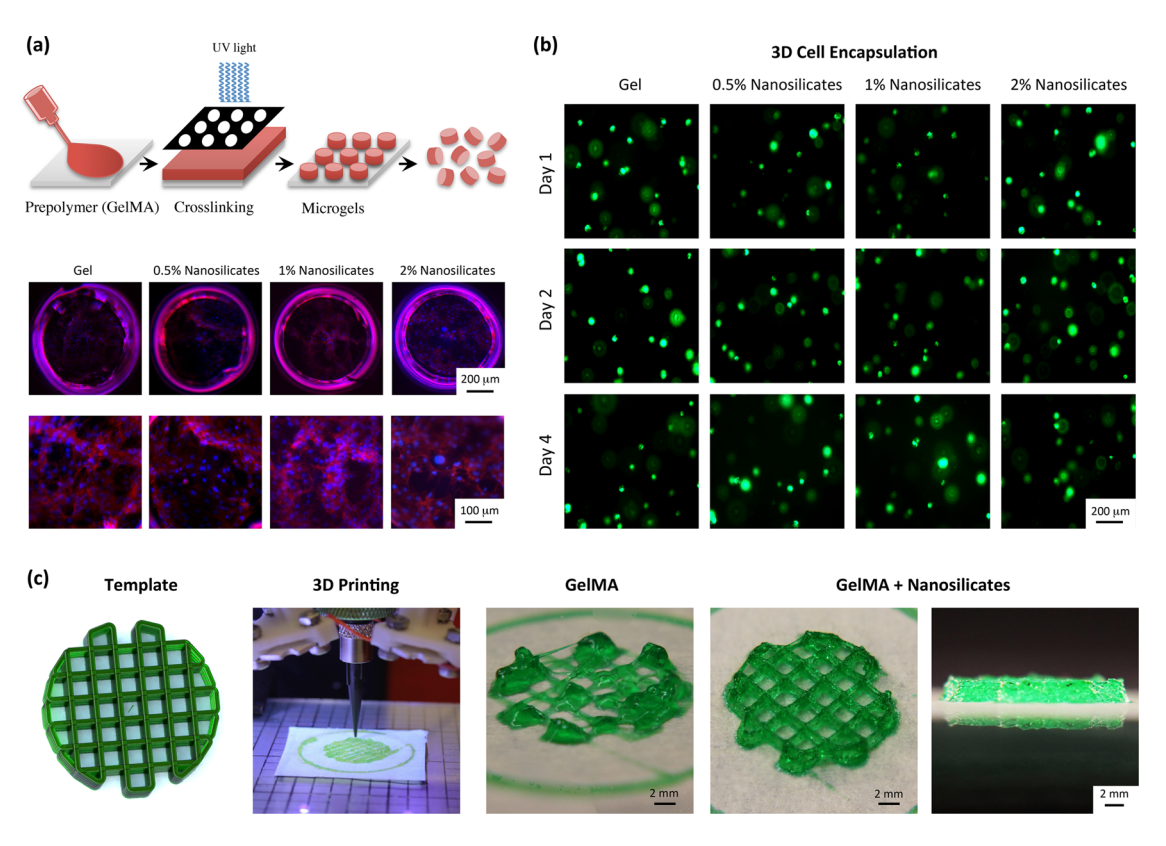


Figure 4. Microfabricated structures from nanocomposite hydrogels. (a) Schematic representation of fabrication of nanosilicate-loaded microgels. Cells readily adhered, elongated, and formed interconnected networks on these microgels, as shown by phalliodin/DAPI images stained for actin filaments and nuclei. (b) In the 3D encapsulation of cells in nanocomposite hydrogels, all scaffolds supported cellular viability, as represented with live/dead images on day 1, day 2, and day 4. (c) The addition of nanosilicate to GelMA (prepolymer) results in a shear-thinning characteristic and can be printed to design complex structures. The printed hydrogels were covalently cross-linked using UV to obtain mechanically stiff hydrogels.

support cell adhesion and proliferation and promote osteogenic differentiation of preosteoblasts in the absence of any osteoinductive factor. Overall, these nanosilicate-based nanocomposites are highly bioactive and show strong promise for use in a range of bone tissue engineering applications.

536

537

538

539

540

541

542

543

544

545

546

547

548

549

550

551

552

553

555

556

557

558

559

560

## **METHODS**

504

505

506

511

512

513

514

515

516

517

518

519

520

521

522

523

524

525

526

527

528

529

530

531

532 533

534

535

Synthesis of Methacrylated Gelatin and Gelatin-Nanosilicate Nanocomposites. Gelatin (type A, from porcine skin) and methacrylic anhydride (MA) were purchased from Sigma-Aldrich, USA. Gelatin methacrylate was synthesized using a previously published method. <sup>21,24</sup> Briefly, a 10% gelatin (w/v) solution in Dulbecco's phosphate-buffered saline (PBS) was prepared at 60 °C. To induce the acrylation of pendent amine groups of the gelatin, methacrylic anhydride (8 mL/10 g gelatin) was added dropwise into the solution while vigorously stirring for 3 h and maintained at 60 °C. The reaction was eventually terminated by addition of excess preheated PBS at 40 °C into the solution. The as-prepared GelMA solution was dialyzed against ultrapure water (18.2  $\Omega$  cm) for a week at 40  $^{\circ}\text{C}$  to remove unreacted methacrylic anhydride and other impurities using a dialysis membrane (mol wt cut off  $\sim$ 12–14 kDa). The solution was then frozen at -80 °C and lyophilized for further characterizations. Nanocomposite hydrogels from GelMA and nanosilicates (also known as Laponite) were prepared at room temperature. The nanosilicates (Laponite XLG) were obtained from Southern Clay Products Inc., USA, and were 25-30 nm in diameter and 1 nm thick. To prepare nanocomposite hydrogels, first the nanosilicates (0, 0.5, 1, and 2 wt %) were dispersed in a photoinitiator solution (0.5 wt % Ciba IRGACURE 2959, Ciba Specialty Chemical, USA) and mixed vigorously for 15 min. Then, GelMA (5 wt %)

was added to the nanosilicate solution and was allowed to disperse for an additional 15 min by vortexing. The prepolymer solution (GelMA and nanosilicates) was cross-linked using UV exposure (320–500 nm) (Omnicure S200, Lumen Dynamics, Canada) for 60 s at an intensity of 6.9 mW/cm². Nanocomposite hydrogels were then soaked in PBS to remove un-cross-linked prepolymer segments.

Physical and Structural Characterization of Nanocomposite Hydrogels. Fourier transform infrared spectra (FT-IR) of the hydrogel were characterized using a Bruker Vector-22 FTIR spectrophotometer (PIKE Technologies, USA). The zeta potential and electrophoretic mobility of the gelatin, nanosilicates, and GelMA-silicate prepolymer solutions were measured at 25 °C using a Zetasizer (Malvern Instruments, UK) equipped with a He-Ne laser. Transmission electron microscopy was performed using a JEOL-JEM 2010 (Japan) at an accelerating voltage of 200 kV on a carbon grid to confirm the size of nanosilicates and interactions between GelMA and nanosilicates. The surface morphology of the nanocomposite hydrogels was evaluated using scanning electron microscopy (FEI Quanta 600 FE-SEM, USA, fitted with an Oxford EDS system) at an accelerating voltage of 20 kV. In brief, to prepare samples for SEM the nanocomposite hydrogels were frozen using liquid nitrogen and then lyophilized for 3 days to obtain dried samples. The dried nanocomposite samples were sputter coated with Au/Pd up to a thickness of 8 nm before

635

636

637

638

639

641

642

643

644

645

646

647

648

649

651

652

653

654

655

656

657

658

659

660

661

662

664

665

666

667

669

670

671

672

673

674

675

676

677

678

679

681

682

683

684

685

686

687

688

689

691

692

693

694

695

696

697

698

699

700

701

702

703

704

705

706

707

being mounted onto the specimen stage for imaging. The pore diameters were analyzed using ImageJ software (National Institutes of Health, USA). Electrophoretic mobility and zeta potentials were measured using a Zetasizer Nano ZS (Malvern Instruments Ltd., USA).

561

562

563

564

565

566

567

568

569

570

571

572

573

574

575

576

577

578

579

580

581

582

583

584

585

586

588 589

590

591

592

593

594

595

596

597

598

599

600

601

602

603

604

605

606

607

608

609

610

611

612

613

614

615

616

617

618

619

620

621

622

623

624

625

626

627

628

629

630

631

632

633

The mechanical properties of the Gel and nanocomposite hydrogels were determined using a mechanical tester (eXpert 7600, ADMET, USA). Hydrogels (n = 6) were incubated in PBS for 24 h before testing. A uniaxial compression test was performed on the cylindrical samples (6 mm  $\times$  2 mm) at a strain rate of 1 mm/min. The compressive modulus was calculated from the slope in the toe region corresponding to 0.10–0.20 strain. The viscoelastic behavior of the hydrogels was evaluated using an MCR rheometer (Anton Paar, USA) equipped with 50 mm flat geometry and a gap of 50  $\mu$ m. Oscillatory strain sweep was performed between 1% and 100% strain at 0.1 Hz frequency at 37 °C. The flow experiment was performed to determine the viscosity of the polymer solution at physiological temperature.

To evaluate the hydration degree of the nanocomposite hydrogels, samples were placed in PBS (varying pH of 3, 7.4, and 10) or in growth media (with and without fetal bovine serum (FBS)) to mimic the biological microenvironment (n = 6). The wet weight  $(M_o)$  of the samples was measured prior to their lyophilization for 24 h to obtain the dried weight ( $M_t$ ). The hydration degrees of the nanocomposite hydrogels are calculated using eq 1:

Hydration degree = 
$$\frac{(M_o - M_t)}{M_o} \times 100$$
 (1)

Nanocomposite hydrogels were subjected to enzymatic degradation by incubating the hydrogels in a collagenase enzyme solution at 37 °C. The enzyme solution was freshly prepared on the day of the experiment using phosphate-buffered saline. The working solution of collagenase (2.5 units/mL) was prepared in PBS from the 300 units/mg collagenase type II enzyme (Worthington Biochemicals, USA). Weight loss was monitored for 4 days, and the percent mass remaining of the nanocomposites was calculated. Further, to determine the protein delivery efficacy of the sample, nanocomposite hydrogels (n = 5) were prepared with 150  $\mu$ L of a prepolymer solution containing 75  $\mu$ g/mL of the fluorescein isothiocyanate labeled bovine serum albumin (FITC-BSA) (Sigma-Aldrich, USA) protein under UV light. The cross-linked nanocomposites with entrapped protein were then incubated in PBS at 37 °C. The amount of protein released was determined by measuring the absorbance of the released protein (2  $\mu L$  of PBS) using a fluorospectrometer (NANODROP 3300, Thermo Scientific, USA) at different time-points over a period of 4 days. More specifically, the protein released was calculated using the absorbance of the protein released from the nanocomposite hydrogels divided by the absorbance of the FITC-BSA protein (75  $\mu$ g). The ability of nanocomposites to facilitate biomineralization was determined by using 10× stimulated body fluid. Nanocomposites prepared by photopolymerization with varying nanosilicate concentrations were immersed in 10× SBF solution for 30 min at 37 °C. Then gels were removed from the SBF solution and washed 3-5 times in distilled water to remove the weakly bound serum from the gel surface. The obtained SBF-coated gels were stained with a 0.5% Alizarin Red S (Sigma-Aldrich, USA) staining for calcium deposits. A stereomicroscope was used to take the images of the hydrogels. Later, the hydrogels were dissolved in a 0.01 M acetic acid solution to dissolve the Alizarin Red S. After centrifuging and neturalizing with 10% (v/v) ammonium hydroxide (Sigma, USA), the amount of Alizarin Red S was quantified by determing the absorbance at 405 nm. One mole of Alizarin Red binds to two moles of calcium in an Alizarin Red S-calcium complex. A calibration curve was obtained from different concentrations of Alizarin Red S in distilled water at pH 4.2, adjusted with 10% (v/v) ammonium hvdroxide.

In Vitro Cell Studies. Preosteoblast cell lines (NIH MC3T3 E1-4, ATCC, USA) were cultured in normal growth media (Alpha MEM, Life Technologies, USA), supplemented with 10% FBS (Life Technologies, USA) and 1% penicillin/streptomycin (100 U/100  $\mu$ g/mL; Life Technologies, USA) at 37 °C with 5% CO<sub>2</sub>. The nanocomposite

hydrogels of 6 mm diameter and 400  $\mu m$  thickness were prepared in 96-well plates. Then, preosteoblast cells were trypisinized and seeded onto the hydrogels at a density of 10000 cells/hydrogel in normal growth media. After 24 and 48 h of cell seeding, the normal media were removed and the hydrogels were washed with PBS. The prepared live/dead assay reagent from Calcein AM and ethidium homodimer (Santa Cruz Biotechnology Inc., USA) were added to the nanocomposites and incubated for 30 min at 37 °C. The samples were washed with PBS three times and imaged using an epifluorescence microscope (TE2000-S. Nikon, USA). The in vitro studies were performed in normal media and osteoconductive media. The osteoconductive media was prepared by supplementing the normal growth media with 10 mM  $\beta$ -glycerophosphate and 50  $\mu$ M ascorbic acid phosphate (Sigma-Aldrich, USA). The metabolic activity of these cells was analyzed using the Alamar Blue assay (Thermo Scientific, USA) in both normal and osteoconductive media on days 0, 1, 3, 7, 10, and 14 using the manufacturer's protocol. The absorbance was recorded using a fluorescence microplate reader (Infinite M200PRO, TECAN, Europe) to obtain the percent reduction in Alamar Blue. The expression of intercellular alkaline phosphatase in preosteoblast cells seeded on the nanocomposite hydrogels in a 48-well plate was evaluated using nitro-blue tetrazolium/indolyl phosphate (NBIT/BCIP) staining (Thermo Scientific, USA). The nanocomposites were washed with PBS and then incubated with 0.25 mL of NBIT/BCIP at 37 °C for 30 min. After incubation, samples were washed with PBS and imaged under bright-field mode using a stereomicroscope (Amscope, USA). The mineralized matrix produced by preosteoblast cells on the nanocomposites was analyzed on days 7 and 14 using Alizaren Red S staining. The cells on the nanocomposite samples were fixed with 2% glutaraldehyde for 15 min and then added with 0.5% Alizarin Red S (pH 4.2; Sigma-Aldrich, USA). After 15 min of incubation, the samples were washed with distilled water to remove the weakly adhered Alizarin Red S, and then imaging was performed. The chemical characteristics of deposited mineral were confirmed by Raman spectra (R200-L SENTERRA Raman microscope) using excitation: 785 and 532 nm (He-Ne laser).

Microfabricated Structures and 3D Encapsulation. To fabricate nanocomposite microgels, 20 µL of prepolymer solution con $taining\,GelMA, nanosilicates, and\,0.25\%\,photoinitiator\,was\,placed$ between glass slides and UV cross-linked using 6.9 mW/cm<sup>2</sup> for 20 s. After cross-linking, the microgels were washed with PBS. seeded with preosteoblasts cells, and incubated in normal media conditions. After 4 days of postseeding the normal media was removed, microgels were washed with PBS, and the cells were fixed using 2% glutaraldehyde solution. The Alexa Fluor 488 Phalloidin (Life Technologies, USA) working solution was added to the microgels at 37 °C for 20 min. The samples were washed with PBS twice followed by the addition of DAPI working solution for 10 min at 37  $^{\circ}\text{C}.$  The samples were washed with PBS three times and were imaged using a fluorescence microscope (Nikon TE2000-S, USA). For cell encapsulation, preosteblast cells with a concentration of  $2 \times 10^5$  cells/mL were added to the prepolymer solution before cross-linking. The crosslinked hydrogels were incubated in normal media conditions. and after 1, 2, and 4 days, the hydrogels were washed with PBS and incubated in live/dead reagent containing Calcein AM and ethidium homodimer (Santa Cruz Biotechnology Inc., USA) for 30 min at 37 °C before imaging.

3D-printed nanocomposite gels were fabricated with fused deposition modeling. Prepolymer solutions containing 8% GelMA (80% methacrylation degree), 0.25% photoinitiator, and 2% nanosilicates, by weight, were mixed at elevated temperature and allowed to cool to room temperature before printing. Solutions were loaded into a HYREL Engine 3D printer equipped with an EMO-25 emulsifiable extruder and a UV blocking, 22 AWG (200  $\mu$ m) tapered dispensing tip (Fisnar). A cylinder model, h = 5 mm, diameter = 20 mm, was used as the physical template for printing. Slic3r v1.1.7 was used to create the g-code for printing. The following settings were used for printing: printing speeds of 5 mm/s, nonprinting speeds of 25 mm/s, layer thickness of 200  $\mu$ m, infill of 50% (0-90°, rectilinear grid), extrusion width of 1.0 mm, and no perimeters, top layers, or bottom layers. Constructs were subjected to UV

781

782

783

784

785

786

787

788

789

790

791

792

793

794

795

796

797

798

799

800

801

802

803

804

805

806

807

808

809

810

811

812

813

814

815

816

817

818

819

820

821

822

823

824

825

826

827

828

829

830

831

832

833

834

835

836

837

838

839

840

841

842

843

844

845

846

847

848

849

850

851

852

853

854

light for the duration of the print (6 min and 50 s). The UV source consists of four UV LEDs (365 nm, 500 mW radiant flux) positioned at a 5 cm vertical distance and 2 cm radial distance from the printing nozzle. After printing, gels were subjected to an additional 5 min of cross-linking under the UV printing source.

**Statistical Analysis.** All the data presented are means and standard deviations of the experiments (n = 5 or 6). Statistical analysis was performed using GraphPad Prism 5 (San Diego, CA, USA). The significant differences between sample groups were determined using the nonparametric test, one-way analysis of variance (ANOVA), and Tukey's *post-hoc* analysis for pairwise mean comparisons. The statistical significance was defined as p < 0.05, \*\*p < 0.01, \*\*\*p < 0.005.

Conflict of Interest: The authors declare no competing financial interest.

Acknowledgment. R.K would like to acknowledge funding support from NSF (CBET 1264848) and NIH (R01 AR066033-01).

Supporting Information Available: Additional data (structural, chemical, and biological characterization of nanocomposite hydrogels) are available free of charge *via* the Internet at http://pubs.acs.org.

# REFERENCES AND NOTES

709

710

711

712

713

714

715

716

717

718

719

720

721

722

723

724

725

726

727

728

729

730

731

732

733

734

735

736

737

738

739

740

741

742

743

744

745

746

747

748

749

750

751

752

753

754

755

756

757

758

759

760

761

762

763

764

765

766

767

768

769

770

771

772

773

774

775

776

777

778

779

- Wegst, U. G. K.; Bai, H.; Saiz, E.; Tomsia, A. P.; Ritchie, R. O. Bioinspired Structural Materials. Nat. Mater. 2015, 14, 23–36.
- Dvir, T.; Timko, B. P.; Kohane, D. S.; Langer, R. Nanotechnological Strategies for Engineering Complex Tissues. *Nat. Nanotechnol.* 2011, 6, 13–22.
- Gaharwar, A. K.; Peppas, N. A.; Khademhosseini, A. Nanocomposite Hydrogels for Biomedical Applications. Biotechnol. Bioeng. 2014, 111, 441–453.
- Carrow, J. K.; Gaharwar, A. K. Bioinspired Polymeric Nanocomposites for Regenerative Medicine. *Macromol. Chem. Phys.* 2015, 216, 248–264.
- Dawson, J. I.; Oreffo, R. O. Clay: New Opportunities for Tissue Regeneration and Biomaterial Design. *Adv. Mater.* 2013, 25, 4069–4086.
- Li, W.; Wang, J.; Ren, J.; Qu, X. 3D Graphene Oxide—Polymer Hydrogel: Near-Infrared Light-Triggered Active Scaffold for Reversible Cell Capture and on-Demand Release. Adv. Mater. 2013, 25, 6737–6743.
- Balazs, A. C.; Emrick, T.; Russell, T. P. Nanoparticle Polymer Composites: Where Two Small Worlds Meet. Science 2006, 314, 1107–1110.
- Bordes, P.; Pollet, E.; Avérous, L. Nano-biocomposites: Biodegradable Ployester/Nanoclay Systems. *Prog. Polym.* Sci. 2009, 34, 125–155.
- Gaharwar, A. K.; Mihaila, S. M.; Swami, A.; Patel, A.; Sant, S.; Reis, R. L.; Marques, A. P.; Gomes, M. E.; Khademhosseini, A. Bioactive Silicate Nanoplatelets for Osteogenic Differentiation of Human Mesenchymal Stem Cells. *Adv. Mater.* 2013, 25, 3329–36.
- Mihaila, S. M.; Gaharwar, A. K.; Reis, R. L.; Khademhosseini, A.; Marques, A. P.; Gomes, M. E. The Osteogenic Differentiation of SSEA-4 Sub-population of Human Adipose Derived Stem Cells using Silicate Nanoplatelets. *Biomater*ials 2014, 35, 9087–9099.
- Gaharwar, A. K.; Avery, R. K.; Assmann, A.; Paul, A.; McKinley, G. H.; Khademhosseini, A.; Olsen, B. D. Shear-Thinning Nanocomposite Hydrogels for the Treatment of Hemorrhage. ACS Nano 2014, 8, 9833–9842.
- Gaharwar, A. K.; Mukundan, S.; Karaca, E.; Dolatshahi-Pirouz, A.; Patel, A.; Rangarajan, K.; Mihaila, S. M.; Iviglia, G.; Zhang, H.; Khademhosseini, A. Nanoclay-Enriched Poly (ε-caprolactone) Electrospun Scaffolds for Osteogenic Differentiation of Human Mesenchymal Stem Cells. Tissue Eng. Part A 2014, 20, 2088–2101.
- Thompson, D. W.; Butterworth, J. T. The Nature of Laponite and Its Aqueous Dispersions. J. Colloid Interface Sci. 1992, 151, 236–243.
- 14. Clément-Lacroix, P.; Ai, M.; Morvan, F.; Roman-Roman, S.; Vayssière, B.; Belleville, C.; Estrera, K.; Warman, M. L.; Baron, R.;

- Rawadi, G. Lrp5-Independent Activation of Wnt Signaling by Lithium Chloride Increases Bone Formation and Bone Mass in Mice. *Proc. Natl. Acad. Sci. U.S.A.* **2005**, *102*, 17406–17411.
- Zhang, F.; Phiel, C. J.; Spece, L.; Gurvich, N.; Klein, P. S. Inhibitory Phosphorylation of Glycogen Synthase Kinase-3 (GSK-3) in Response to Lithium Evidence for Autoregulation of GSK-3. *J. Biol. Chem.* 2003, 278, 33067–33077.
- Clevers, H. Wnt/β-Catenin Signaling in Development and Disease. Cell 2006, 127, 469–480.
- Ruzicka, B.; Zaccarelli, E.; Zulian, L.; Angelini, R.; Sztucki, M.; Moussaïd, A.; Narayanan, T.; Sciortino, F. Observation of Empty Liquids and Equilibrum Gels in a Colloidal Clay. *Nat. Mater.* 2011, 10, 56–60.
- Angelini, R.; Zaccarelli, E.; de Melo Marques, F. A.; Sztucki, M.; Fluerasu, A.; Ruocco, G.; Ruzicka, B. Glass—Glass Transition during Aging of a Collodial Clay. Nat. Commun. 2014, 5, 4049.
- Bonn, D.; Tanase, S.; Abou, B.; Tanaka, H.; Meunier, J. Laponite: Aging and Shear Rejuvenation of a Colloidal Glass. Phys. Rev. Lett. 2002, 89, 015701.
- Wang, Q.; Mynar, J. L.; Yoshida, M.; Lee, E.; Lee, M.; Okuro, K.; Kinbara, K.; Aida, T. High-Water-Content Mouldable Hydrogels by Mixing Clay and a Dendritic Molecular Binder. Nature 2010. 463, 339–343.
- Nichol, J. W.; Koshy, S. T.; Bae, H.; Hwang, C. M.; Yamanlar, S.; Khademhosseini, A. Cell-Laden Microengineered Gelatin Methacrylate Hydrogels. *Biomaterials* 2010, 31, 5536–5544.
- Mũnoz, Ž.; Shih, H.; Lin, C.-C. Gelatin Hydrogels Formed by Orthogonal Thiol—Norbornene Photochemistry for Cell Encapsulation. *Biomater. Sci.* 2014, 2, 1063–1072.
- García, A. J. Get a Grip: Integrins in Cell—Biomaterial Interactions. Biomaterials 2005, 26, 7525–7529.
- Benton, J. A.; DeForest, C. A.; Vivekanandan, V.; Anseth, K. S. Photocrosslinking of Gelatin Macromers to Synthesize Porous Hydrogels that Promote Valvular Interstitial Cell Function. *Tissue Eng. Part A* 2009, 15, 3221–3230.
- Annabi, N.; Nichol, J. W.; Zhong, X.; Ji, C.; Koshy, S.; Khademhosseini, A.; Dehghani, F. Controlling the Porosity and Microarchitecture of Hydrogels for Tissue Engineering. Tissue Eng. Part B 2010, 16, 371–383.
- Shin, S. R.; Jung, S. M.; Zalabany, M.; Kim, K.; Zorlutuna, P.; Kim, S. b.; Nikkhah, M.; Khabiry, M.; Azize, M.; Kong, J. Carbon-Nanotube-Embedded Hydrogel Sheets for Engineering Cardiac Constructs and Bioactuators. ACS Nano 2013, 7, 2369–2380.
- Wang, Q.; Hou, R.; Cheng, Y.; Fu, J. Super-Tough Double-Network Hydrogels Reinforced by Covalenty Compositing with Silica-Nanoparticles. Soft Matter 2012, 8, 6048–6056.
- Hule, R. A.; Pochan, D. J. Polymer Nanocomposites for Biomedical Applications. MRS Bull. 2007, 32, 354–358.
- Shin, S. R.; Aghaei-Ghareh-Bolagh, B.; Dang, T. T.; Topkaya, S. N.; Gao, X.; Yang, S. Y.; Jung, S. M.; Oh, J. H.; Dokmeci, M. R.; Tang, X.; Khademhosseini, A. Cell-Laden Microengineered and Mechanically Tunable Hybrid Hydrogels of Gelatin and Graphene Oxide. Adv. Mater. 2013, 25, 6385–6391.
- Cha, C.; Shin, S. R.; Gao, X.; Annabi, N.; Dokmeci, M. R.; Tang, X. S.; Khademhosseini, A. Controlling Mechanical Properties of Cell-Laden Hydrogels by Covalent Incorporation of Graphene Oxide. Small 2014, 10, 514–523.
- Kokubo, T.; Takadama, H. How Useful Is SBF in Predicting in Vivo Bone Bioactivity? Biomaterials 2006, 27, 2907–2915.
- Rhee, S. H.; Lee, J. D.; Tanaka, J. Nucleation of Hydroxyapatite Crystal through Chemical Interaction with Collagen. J. Am. Ceram. Soc. 2000, 83, 2890–2892.
- Gregory, C. A.; Grady Gunn, W.; Peister, A.; Prockop, D. J. An Alizarin Red-Based Assay of Mineralization by Adherent Cells in Culture: Comparison with Cetylpyridinium Chloride Extraction. Anal. Biochem. 2004, 329, 77–84.
- 34. Murphy, S. V.; Atala, A. 3D Bioprinting of Tissues and Organs. *Nat. Biotechnol.* **2014**, *32*, 773–785.
- Schuurman, W.; Levett, P. A.; Pot, M. W.; van Weeren, P. R.; Dhert, W. J.; Hutmacher, D. W.; Melchels, F. P.; Klein, T. J.; Malda, J. Gelatin-Methacrylamide Hydrogels as Potential Biomaterials for Fabrication of Tissue Engineered Cartilage Constructs. *Macromol. Biosci.* 2013, 13, 551–561.